
Shelf-edge jet currents in the southern Benguela: a modelling approach

Veitch Jennifer ^{1,*}, Hermes Juliet ¹, Lamont Tarron ^{2,3}, Penven Pierrick ⁴, Dufois Francois ⁵

¹ South African Environmental Observation Network, Egagasini Node, Private Bag X2, Roggebaai 8012, South Africa

² Oceans & Coasts Research Branch, Department of Environmental Affairs, Private Bag X4390, Cape Town, 8000, South Africa

³ Marine Research Institute and Department of Oceanography, University of Cape Town, Private Bag X3, Rondebosch, 7701, South Africa

⁴ Laboratoire des Physique des Oceans (UMR 6523 CNRS, IFREMER, IRD, UBO), Brest, France

⁵ ARC Centre of Excellence for Coral Reef Studies, University of Western Australia, Crawley WA 6009, Australia

* Corresponding author : Jennifer Veitch, email address : jenny@saeon.ac.za

Abstract :

The dynamics and seasonal variability of jet currents on the southern Benguela shelf-edge are investigated using a climatologically forced ROMS model. The jet is primarily forced by the intense horizontal gradients that exist across the southern Benguela shelf. These gradients are set up by nearshore cooling via the strongly seasonal upwelling regime and variable offshore warming by the advection of Agulhas waters. While the nearshore cooling is prevalent only during the spring and summer upwelling season, the offshore warming exists throughout the year. As a result intensified geostrophically adjusted currents exist throughout the year, particularly off the Cape Peninsula and Cape Columbine. However, the distinct shelf-edge jet features are most intense during upwelling seasons and extend, more or less continuously, from Cape Agulhas, the southern-tip of the continent, to Cape Columbine. The spring and summer jet off the Cape Peninsula reaches speeds of at least 0.7 m.s⁻¹, bifurcates as it moves northward. The branch that continues northward over the shelf goes on to feed the offshore branch of the Cape Columbine jet (over the 500 m isobath) and to a less extent the nearshore branch (over the 200 m isobath) that is locally enhanced by upwelling processes. During winter, the CP jet is more confined to the shelf region and goes on to feed the whole outer-shelf (200-500 m) region off and beyond Cape Columbine. An ageostrophic component associated with offshore non-linearities related to Agulhas influx causes the mean manifestation of the Cape Peninsula jet to broaden slightly (60 km) compared to its 40 km-wide geostrophic core which is situated over the 350 m isobath. The ageostrophic component is related to the generation of eddies that cause the isopycnals to flatten out.

Highlights

► The intense cross-shelf density gradient drives jet currents in the S. Benguela. ► The seasonal variability of the density gradient is controlled by coastal upwelling. ► The gradient is modulated by variability linked to the warm offshore Agulhas waters.

Keywords : Southern Benguela, Shelf-edge jet, Numerical model

1. Introduction

The intense jet currents over the shelf between the Cape Peninsula and Cape Columbine, variously known as the Goodhope jet or the Benguela jet, have been extensively studied over the years due to their role in transporting sardine and anchovy eggs and larvae from their spawning ground on the Agulhas Bank to their nursery area in St. Helena Bay (Shelton and Hutchings (1982), Fowler and Boyd (1998)). More recently, Stenevik et al. (2008) concluded that two different hake species also use the jet current for the transport of fish eggs and larvae. After the spawning of eggs, they need to be entrained into the jet current where they hatch on the way to their nursery ground (Mullon et al., 2003). Therefore, to ensure successful recruitment there needs to be a coupling between the hatching of eggs and the jet current. The shelf-edge jet currents are thus crucial to the successful fishing industry off the South African west coast.

Given the intense horizontal gradients in the region the jet was anticipated and later discovered by Bang and Andrews (1974) and has been described by Shannon and Nelson (1996) as a convergent NW-oriented current system on the western Agulhas Bank that funnels into the west coast and bifurcates at Cape Columbine into an offshore and alongshore component. It is 20-30 km wide,

has characteristic speeds of 0.5 m.s^{-1} and is located over the steep shelf in the region. While Nelson and Hutchings (1983) observed that the jet is permanently present, irrespective of wind conditions, Boyd and Nelson (1998) found that the highly seasonal coastal upwelling regime (intense upwelling in austral summer) plays a key role in its location and intensity, which can reach speeds of $0.5\text{-}0.75 \text{ m.s}^{-1}$ (Boyd and Oberholzer, 1992) during the peak upwelling season. Huggett et al. (1998) confirmed that the speed of the jet is dependant on the strength of upwelling favourable winds and van der Lingen and Hugget (2003) noted that it exists between the 200-500 m isobaths and frequently varies between them. From satellite altimetry, Strub et al. (1998) similarly noted a seasonal strengthening of the jet, which they associated with the injection of water of high steric heights, via Agulhas influx on the offshore side of the jet and upwelled water on the inshore side of the jet and that it is strongest and closest to the coast during the upwelling season. The enhancement of the jet by the Agulhas influx was corroborated in a model experiment by Veitch (2009) who compared the model-derived jets in a simulation with and without the influence of the Agulhas. Due to the relevance of the jet in the recruitment of sardine, anchovy and hake the SARP (sardine and anchovy recruitment program) monitoring line was established in 1995, extending 55 km southwestward off the Cape Peninsula, taking measurements once a month if possible. While the data provides useful insight into the general characteristics of the jet, a seasonal cycle is difficult to establish given that data was not collected for all months (at least 2 months per year are missing and not always the same months) and that each transect represents a pseudo-'snapshot'. Despite this, the *in situ* data shows that the jet is deep, situated at the shelf-edge and has typical speeds of about 0.75 m.s^{-1} during summer and is broader and shallower with speeds of about 0.5 m.s^{-1} during winter (J.Butler, 2012). Fig. 1 shows the meridional and zonal currents along the SARP line for 30 November 2015 and, a day later on the 1 December 2015. An intense, 40 km wide, northwestward current is clearly evident in the vicinity of the shelf-edge, the core of which is centered over the 350 m isobath. It almost reaches the bottom, but narrows and weakens with depth.

Inshore of the jet is a barotropic alongshore poleward current that was also observed by Nelson (1985). A day later, the shelf-edge jet feature has diminished significantly and the nearshore barotropic poleward flow has taken on a more westward component. While the *in situ* data gives us an idea of the intensity and location of the jet as well as the fact that it can significantly diminish within a day, it fails to provide a spatial or temporal context. In this paper we make use of a climatological model experiment in order to investigate the dynamics and seasonal variability of the shelf-edge jets between the Cape Peninsula and Cape Columbine. The role of Agulhas influx on the jet currents is addressed by making use of a model experiment in which the impact of the Agulhas has been effectively removed from the Benguela system (refer to Veitch and Penven (2017) and Chang (2009)), an analysis of the cross-shelf heat budget for both simulations (with and without the Agulhas) allows for a better understanding of the development of the intense cross-shelf thermal gradient associated with the jet currents and the Ichthyop lagrangian transport tool (Lett et al., 2008) is used to better visualize jet bifurcation and the connectivity between the jets off the Cape Peninsula and Cape Columbine.

2. Data and Methods

2.1. Hydrodynamic model configuration

The Regional Ocean Modelling System (ROMS) is a split-explicit, free-surface, topography-following vertical coordinate model that is well suited for regional applications (Shchepetkin and McWilliams, 2005, 2008; Haidvogel and Beckmann, 1999). It solves the incompressible primitive equations based on the Boussinesq and hydrostatic approximations and is coupled to advection-diffusion schemes for potential temperature and salinity as well as a non-linear equation of state for density. The advection scheme is third-order upstream biased, which reduces dispersion errors, essentially enhancing precision for a given grid resolution (Shchepetkin and McWilliams, 1998). However, the implementation of the third-order advection-diffusion scheme has lead to the development of spurious

diapycnal mixing in sigma-coordinate models. A solution to this problem was addressed by Marchesiello et al. (2008) and involves the split of advection and diffusion, the latter of which appears as a biharmonic operator. This solution was implemented in our configuration in order to preserve the low diffusion and dispersion benefits of the original scheme while maintaining water mass characteristics. Explicitly prescribed lateral viscosity is zero everywhere except in sponge layers at open boundaries, where it increases smoothly toward the edge of the domain. Open boundary conditions of the parent domain are a combination of outward radiation and nudging toward prescribed external boundary conditions and are described by Marchesiello et al. (2001). Subgrid-scale vertical mixing is introduced by the nonlocal K-profile parameterization (KPP) scheme (Large et al., 1994). The bottom boundary layer is generated by a KPP bottom drag. The bottom friction coefficient is calculated through the use of a logarithmic boundary layer formulation with a bottom roughness of 10 cm.

In order to maximize computing efficiency, the Adaptive Grid Refinement in Fortran (AGRIF) two-way nesting capability (Debreu et al., 2008) of ROMS was employed in which the boundaries of a higher resolution child domain are provided by a lower resolution parent domain within which the child is embedded. The two-way nesting scheme provided the parent-child feedback, as deemed necessary in this region where large-scale Agulhas rings traverse from child to parent domain. The topography of the nested configuration is based on the 1' General Bathymetric Chart of the Oceans (GEBCO; available online at <http://www.gebco.net>). Both the parent and child domains have 32 topography-following vertical levels that are stretched toward the surface. The parent domain is known as the Southern African Experiment (SAfE) and was designed by Penven et al. (2006) to capture salient southern African oceanographic features. The domain encompasses the region spanning 2.5°W-54.75°E and 46.75°S-4.8°S and has a horizontal resolution that ranges from 19 km in the south to 27.6 km in the north. The child domain encompasses the greater Benguela system, inclusive of both the nearshore upwelling regime as well as the large-scale offshore current domain, spanning 3.9°E-19.8°E and 35.6°S-12.1°S

and has a horizontal resolution that ranges from 9 km in the north to 7.5 km in the south. The model is forced with a 0.5° QuikSCAT climatological wind forcing, based on data spanning 2000-2007, and surface heat and salt fluxes from the Comprehensive Ocean-Atmosphere Data Set (COADS) climatologies (Da Silva et al., 1994). Initialization was from a state of no-flow and mean January temperatures and salinities from the World Ocean Atlas 2005 (WOA; Conkright et al. (2002)). ROMS addresses the lack of an atmosphere-ocean feedback term and the potential therefore of the model SSTs to drift by the parameterization of a linearized atmosphere-ocean feedback term for the surface heat flux. This SST 'restoring' is done using the 9 km Pathfinder climatological SST product and a similar surface salinity correction scheme is applied using the COADS climatological data due to the paucity of evaporation-precipitation forcing data. The nested configuration is run for 10 years, of which the first two are considered the spin-up period after which the model solution reaches statistical equilibrium when a robust seasonal signal approximately repeats itself and no temporal drift is evident. The boundary conditions for the parent domain are supplied by WOA 2005 (Da Silva et al., 1994) temperatures and salinities from which geostrophic velocities are calculated, together with the QuikSCAT climatological wind stresses for Ekman transports. In order to explicitly show the impact of the Agulhas on the shelf-edge jets, this configuration (REF) has been rerun but with the Agulhas removed (NOA) by altering the land mask to include a dam off Durban so that the Agulhas is diverted eastward and does not directly influence the southern Benguela (Chang (2009) and Veitch and Penven (2017)). The REF model simulation has been used in Veitch et al. (2009) and Veitch et al. (2010) and both the REF and NOA simulations have been used in Veitch and Penven (2017) where more information can be found on the configurations. Extensive model-data comparisons have been presented by Veitch et al. (2009), Veitch (2009) and Veitch et al. (2010) showing that the model is reproducing the known aspects of the ocean circulation in the region.

2.2. Lagrangian drifter configuration

The Ichthyop individual based model (Lett et al., 2008) is used in order to visualize the connectivity of shelf-edge jets in the southern Benguela system. 10 000 particles are released from a 20 km radius, 20 m deep region centered between the 200 - 500 m isobaths off the Cape Peninsula every second day for all months of model years 6 - 8. The locations of all the drifters, as well as their median locations, per day after release are plotted separately for summer and winter months in order to get a sense of the seasonal variability in the nature and connectivity of the shelf-edge jets.

2.3. Satellite data

The AVISO absolute dynamic topography was used for comparisons of model and satellite EKE. The $\frac{1}{3}^\circ$ gridded product is compiled from data spanning October 1992-September 2008. The product is the sum of Rio5 (Rio et al. (2005)) satellite sea level anomalies and the mean dynamic topography. While AVISO gridded data products provide a rich data source from which to compare model output, it is not reliable within a 50 km coastal band. The satellite sea surface temperature (SST) product used is Level-2 Moderate Resolution Imaging Spectroradiometer (MODIS) data from NASAs TERRA satellite that has been processed at a 4 km resolution (Dufois et al. (2012)) and compiled into climatologies and regridded onto the model grid of the southern Benguela region.

3. Results and Discussion

3.1. Surface manifestation of shelf-edge jet currents

The spatially and temporally cohesive model output allows for a complete view of the southern Benguela jet currents and in this paper we split the year into two 6-monthly averages that represent the upwelling and no-upwelling periods: October-March (we will call it austral summer) and April-September (austral winter). Summer and winter mean surface current speed and direction (Fig.

2) show that off Cape Columbine (CC) and the Cape Peninsula (CP), a shelf-edge intensification of the currents exists throughout the year. During winter months the jet is limited to seemingly more isolated features off CC and CP and is much stronger during austral summer months, existing from as far south as Cape Agulhas with speeds in excess of 0.4 m.s^{-1} throughout the shelf-edge region to CC. The jet is therefore a permanent feature between the 200-500 m isobaths off CP, that is significantly amplified during upwelling seasons, which is consistent with the findings of Nelson and Hutchings (1983), Nelson (1985) and Boyd and Nelson (1998). We will call this jet the Cape Peninsula (CP) jet in order to distinguish it from the intensified current off CC. The CP jet is locally enhanced during periods of active upwelling, but is also fed from the south by the jet associated with summer upwelling at CA as well as the large-scale geostrophic currents associated with cross-shelf density gradient throughout the year. The shelf-edge broadens off CC, with an intensification of the currents over the 200 m isobath throughout the year that is more intense during summer. A secondary and much weaker jet-like feature occurs over the 500 m isobath off CC during summer months only. The divergent jet-like feature off CC during summer months has been described by Shannon and Nelson (1996) and recently confirmed by climatological hydrographic measurements Lamont et al. (2015). During winter the distinct 'double' jet feature off CC does not exist, which has similarly been confirmed by hydrographic data in this region that shows only a single front (the CC front) during winter (Lamont et al., 2015). Instead, the nearshore portion of the CP jet veers northward toward the coast just north of the Cape Peninsula while the offshore portion continues northward along the shelf-edge. These distinct streams converge off CC, enhancing the jet feature that exists there during winter.

While there is *in situ* data available that captures the jet off Cape Point, the data is limited to either a mooring in one or two locations for a few months at a time or to a transect sampled monthly or quarterly across the jet (see Fig 1). Neither of these provides a complete record of the structure and variability of the jet in space or time. Using the available data to evaluate the model

therefore needs to be done cautiously, especially given that the model is somewhat idealised as it uses climatological winds. Despite this, the several available cross-shelf transects allow us to confirm that the mean position of the model jet, situated between the 200-500 m isobaths off CP, is realistic (see Fig. 1). For a more explicit evaluation of the ability of the model to capture the shelf-edge jet features we appeal to the premise that they are predominantly driven by cross-shelf sea surface temperature (SST) gradients. Comparing model and satellite SST (Fig. 3), we note that the general pattern of cooler water nearshore, particularly during the summer upwelling season, and warmer water offshore, particularly in the southeast of the domain in connection with Agulhas influx, is captured by the model. However, the model does present some SST biases (not shown): offshore of the 200 m isobath there is a persistent warm bias that ranges from less than 0.5°C in the northern part of the domain, over the shelf-edge and is in excess of 2°C in the southeast corner of the domain. The model also fails to capture smaller-scale intricacies associated with the intense SST gradients over the shelf. In order to delineate the approximate position of the jet features in relation to SSTs, overlaid on the seasonal mean model and satellite SST plots is the $0.40 \text{ m}\cdot\text{s}^{-1}$ model isotach. The jet features coincide with most intense model and satellite SST gradients, suggesting that they may indeed be driven by cross-shelf SST gradients and that the latter can be used as a proxy for the geostrophically adjusted portion of the jet.

To explore the seasonal variability of the intense SST gradient in more detail, Fig. 4 shows the monthly mean SST gradient, computed as the east-west SST difference between adjacent model grid points or satellite data pixels, across the CP jet at 34.14°S , from the coast to beyond the shelf-edge, based on model and satellite data. The approximate positions of the 200 and 500m isobaths, within which the CP jet tends to be confined, are represented by the bold black lines. Within this region, the gradient values range between -0.02 to $-0.1 \text{ }^{\circ}\text{C}\cdot\text{km}^{-1}$ for both model and satellite data, with highest values during the upwelling season from October to March. While the model successfully captures the timing and general offshore extent of the most intense temperature gradient, it dampens

the variability within the shelf-edge region, simulating a much more steady front in both space (in terms of width and offshore extent) and time.

The corresponding, model-derived surface alongshore (i.e. parallel to the coast) current speed and alongshore windstress at the coast (Fig. 5) reveals that the most intense jet is coincident with strongest upwelling-favourable winds and most intense SST gradient. A slightly enhanced negative SST gradient exists over the shelf-edge region even during months when the coastal winds are either very weakly upwelling favourable or weakly downwelling favourable (see Fig. 5), suggesting that a source of enhanced offshore warming is responsible for its maintenance. This heat contribution is provided by Agulhas influx. Using the SST gradient as a proxy for the CP jet, the satellite data shows that it is narrower and intensified toward the 200 m isobath during the first half of the upwelling season (October-December) and is a broader and more intense feature during the second half of the upwelling season (January-March) than is reproduced by the model. The good match of SST gradient during winter gives confidence that the weaker winter jet is reproduced by the model.

3.2. *The cross-shelf density gradient*

In order to determine to what extent the CP jet is driven by the cross-shelf density gradient, of which the cross-shelf temperature gradient can be thought of as a proxy, we reproduce the vertical structure of the jet using the thermal wind relationship (see equation 1) and surface geostrophic velocities as the reference from which we integrate. The thermal wind relationship describes the connection between the cross-shelf gradient in density and the shear in the alongshore current. We derive the geostrophic velocities in this manner for both the REF and NOA model simulations so that we can more quantitatively assess the role of the Agulhas in the intensification of the jet current.

$$-\frac{g}{f\rho_0}\frac{\partial\rho}{\partial x} = \frac{\partial v}{\partial z} \quad (1)$$

where g is the acceleration due to gravity, ρ is the density of seawater, ρ_0 is the reference density of seawater, f is the coriolis parameter and v is the

meridional velocity component. Surface, model-derived geostrophic velocities are used as the reference level for v . In Fig. 6 the model-derived alongshore velocity (total) is shown alongside the density field, the thermal wind-derived velocity (geostrophic) and the ageostrophic (total minus geostrophic) alongshore velocity. For the REF simulation, the peak velocities are well reproduced by the thermal wind relationship as is the location of the core of the jet, between the 250-300 m isobaths. This underscores the essential role that the offshore density gradient (and, by proxy, the temperature gradient) has in driving the intense shelf-edge jet currents. However, the thermal wind relationship only reproduces the geostrophic component of the jet. The jet reproduced by the model is a less-intense, broader feature that is shallower over the shelf (inshore of the 500 m isobath) region: the former can be attributed to the offshore non-linear, ageostrophic components associated with Agulhas influx and the latter to the fact that the thermal wind equation does not take into account bottom friction that acts to oppose the alongshore current. Evidence of intense nonlinearities associated with Agulhas influx can be seen in the extremely high eddy kinetic energies in the REF simulation as opposed to the NOA experiment as well as much higher root mean square errors of the velocity sections (not shown), particularly just offshore of the shelf-edge in the REF simulation. The grey lines in the top, fourth panel of Fig. 6 represent the negative alongshore ageostrophic component of the CP jet in the REF simulation. Their existence just offshore of the core of the jet and further offshore to a depth of about 300 m is consistent with the broadening of the geostrophic jet and is related to instabilities associated with the intense density gradient as well as to instabilities associated with Agulhas influx that cause the jet to slow down.

While the model-derived jet has a very distinct vertical shear, a significant correlation exists at the 95% level ($R=0.91, p<0.001$) between the upper (0-50 m) and lower (50-500 m) jet transport values, suggesting that the barotropic component of flow is strong and justifying the use of only the surface manifestation of the front for analysis.

It has been established that the jet is driven by the intense offshore density

gradient that is set up, on one hand, by the cold summer upwelled waters in the nearshore region and on the other, by the warm offshore region associated with year-round Agulhas influx. In order to explicitly show how the warm waters associated with Agulhas influx affect the jet, we rerun our climatological model simulation but remove the direct influence of the Agulhas in the Benguela system (Chang (2009) and Veitch and Penven (2017)). The thermal-wind recreation of the jet using the density field from the NOA experiment (Fig. 6, bottom) matches the structure of the model-derived NOA better than in the simulation in which the Agulhas is included (REF), other than it being slightly deeper due to the lack of bottom friction in the thermal wind reconstruction and weaker on its offshore flank due to a negative ageostrophic component associated with jet instabilities. This experiment explicitly shows that the geostrophic component of the jet is enhanced and slightly widened by the Agulhas influx in the offshore domain, but it is also further evidence that the very broad jet feature in the REF simulation that is not fully resolved by the thermal wind relationship is the result of non-linearities associated with instabilities associated with both the upwelling jet, as is the case in the NOA experiment, as well as Agulhas influx. Evidence of the latter exists in the fact that the ageostrophic component for the REF simulation extends to the offshore end of the section to depths of at least 300 m, but for the NOA experiment it does not.

Evidence of the extreme variability and importance of non-linearities in the offshore domain of the southern Benguela can be seen in Fig. 7, which shows the surface eddy kinetic energy, a measure of mesoscale variability, for the REF and NOA simulations as well as derived from satellite altimetry. Note that we use the term 'eddy' not to exclusively describe coherent cyclonic or anticyclonic eddy features, but rather as general deviations from the seasonal-mean state. Because our model is forced with monthly mean climatological winds, the mesoscale variability captured by the EKE, can be clearly defined as intraseasonal variability. The high offshore values in the REF simulation is in good agreement with satellite values, even though the model is forced with climatological mean winds. The implication of this is that much of the variability

in the offshore Benguela region is intrinsic rather than forced. The high EKE captured by the model over the shelf-edge and not by the satellite is due to be the result of the low resolution of the gridded satellite altimeter product and their consequent inability to capture nearshore features and instabilities associated with them, especially in regions where the shelf is narrow, like off CP. The very high EKE over the shelf in the REF simulation is both locally produced by instabilities associated with the intense shelf-edge jet currents and remotely influenced: directly, by the advection of mesoscale features associated with Agulhas influx and indirectly by the enhancement of the jet, which in turn enhances local instabilities. For the NOA experiment highest EKEs are associated with the CP and CC jet currents as well as a region extending offshore of a prominent bend in the 500m isobath at 33.5°S. Given that the offshore domain, dominated by high variability associated with Agulhas features, significantly modifies the cross-shelf density gradient that drives the jet, we expect a dampening of the seasonal signal of the CP jet.

We hypothesize therefore that the shelf-edge jets are the geostrophically adjusted currents associated with the highly seasonal upwelling front and that they are geostrophically and ageostrophically enhanced and modulated by the warm Agulhas influx and intense mesoscale variability associated with it. Because Agulhas influx results in an offshore warming throughout the year, the jet is persistent but is amplified during the summer upwelling season. Comparing a timeseries of 2-daily across-shelf averaged (between the locations of the 200-500 m isobaths) alongshore velocity for both the REF and NOA simulations along 34.14°S, both forced with climatological winds, shows this clearly (Fig. 8), for the full 8 year period. It is immediately clear from the timeseries that Agulhas influx results in a generally much faster and more variable CP jet. A significant correlation at the 95% level exists between the NOA CP jet and the alongshore coastal wind stress ($R=0.75, p=0.05$), while the correlation of the latter with the REF CP jet is weak ($R=0.18, p=0.05$). The power spectrum density plots (Fig. 8c) show that there is a significant peak signal at the annual cycle for only the NOA CP jet (solid grey line) and that there is no

clearly significant signal for the REF CP jet (solid black line), but that there is increased power within the 2-3 cycles per year, or 4-6 month period, band. As well as an annual signal associated with wind-driven upwelling, this 4-6 month signal is significant in the nearshore (inshore of the 200 m isobath) sea surface height (SSH) signal for both the REF and NOA simulations (see the dashed black and grey spectral signals in Fig. 8c). The 4-6 month periodicity present in the nearshore SSH signal is in response to the development of cyclonic eddies within the CP upwelling regime. These eddies have been observed via both in situ (Lutjeharms and Stockton, 1987; Lutjeharms and Mathysen, 1995) and satellite (Strub et al., 1998) data. They have been shown to develop within the cool upwelling regime (Strub et al., 1998) and not to be related to changes in the wind field (Lutjeharms and Mathysen, 1995) or to have a seasonal signal (Lutjeharms and Stockton, 1987). The fact that evidence of them exists in the SSH signals of both the REF and NOA simulations suggest that their formation is not dependant on features associated with Agulhas leakage. Notwithstanding the strongly seasonal cycle of the upwelling regime and associated offshore density gradient, these results show that the modulation of the gradient by the remote influence of Agulhas influx that is manifested as a highly turbulent offshore regime and, to some degree, nearshore intrinsic variability results in an extremely variable CP jet.

3.2.1. Heat budget

Given that the shelf-edge jets are primarily driven by the cross-shelf density front and therefore strong temperature gradients, we investigate the thermodynamics of the region by analysing the upper-ocean (0-100m) heat budget across the shelf-edge, averaged alongshore between the CP and CC jets. While the process of frontogenesis and the maintenance of thermal fronts involves more terms than are present in the temperature equation (Hoskins, 1982), the latter is sufficient to provide useful information at our scale of interest. We look at the time-mean (zero tendency term), upper ocean (0-100 m) integrated heat budget (equation 2) for both the REF and NOA simulations in order to assess the

role of Agulhas influx in the cross-shelf thermal gradient. The parameterized sub-grid scale diffusion term is neglected as it is small in this time-mean and relatively deep integrated solution. The total heat flux terms are split into their mean and eddy parts (equation 3) in order to evaluate their roles in the thermal gradient across the shelf edge. The eddy terms are derived by subtracting the total from the seasonal mean values, which means that it resolves intraseasonal variations.

$$0 = - \int_{z_0}^{\eta} \mathbf{u} \cdot \nabla T + Q \quad (2)$$

$$0 = - \int_{z_0}^{\eta} \nabla \cdot \bar{\mathbf{u}} \bar{T} - \int_{z_0}^{\eta} \overline{\nabla \cdot \mathbf{u}' T'} + Q \quad (3)$$

where T is the temperature, η is the surface elevation, z_0 is the bottom level from which we integrate (100m), Q is the ocean-atmosphere heat flux and \mathbf{u} is the 3D velocity. The first term on the RHS of equation 2 represents the depth integrated heat flux advection terms and in equation 3 it is separated into its mean (\bar{T} and $\bar{\mathbf{u}}$) and eddy (T' and \mathbf{u}') components respectively. We are interested in the role of the total, mean and eddy advection terms on heating across the shelf region and how the contributions from each differ in the REF and NOA simulations.

The cross-shelf profile of the depth-integrated total heat advection term for the REF simulation looks very different from the NOA experiment (Fig. 9a) in that it is responsible for monotonically increasing warming from the position of the 350 m isobath (we will call it the mid-shelf) toward the offshore direction in the former, but it is responsible for cooling everywhere, particularly so in the nearshore upwelling domain in the case of the latter. In the case of the REF simulation, the cooling inshore of the mid-shelf associated with the upwelling regime, alongside the warming that occurs offshore of this is consistent with the intense cross-shelf temperature gradient that occurs over the shelf and drives intense jet currents. Separating the total advection term into its mean and eddy components, the latter describing intrinsic intraseasonal variability (Fig

9b), we note that the net warming offshore of the mid-shelf region in the REF simulation is dominantly driven by eddy fluxes with a, not insignificant, mean component compensating by causing cooling in the offshore domain. Inshore of the mid-shelf, the mean component dominates the net cooling signal with smaller heating contributions from the eddy terms. On the other hand, in the NOA experiment, the net cooling is dominated by the mean component, while the eddy contribution is negligible.

This heat budget analysis has provided further evidence that the intense jet between the 200 and 500 m isobaths is driven by a thermal gradient that is driven by highly variable offshore warming associated with Agulhas influx juxtaposed against the highly seasonal nearshore cooling associated with the upwelling regime.

3.3. Jet bifurcation and connectivity between the CP and CC jets

Fig. 2 clearly shows that intensified jets exist off both CP and CC throughout the year. During summer, the upwelling season, the jets are more intense and off CC there is a 'double' jet-feature: the inshore branch centered over the 200 m isobath and the offshore branch over the 500 m isobath. In winter the offshore jet-feature is not present, but there is an intensification between the 200-500 m isobaths north of CC. The extent to which the CP jet bifurcates and/or feeds either the nearshore or offshore jets off CC is not clear. In this section we analyse cross-shelf volume fluxes and run lagrangian drifter experiments to investigate the connectivity between the CP and CC jets.

As a first approach at understanding the possible bifurcation of the CP jet, we look at the summer and winter mean cross-shelf volume transport integrated over the full depth and in 0.2° alongshore bins where positive values refer to offshore transport (Fig. 10). In the context of this analysis we have chosen 'shelf' to be the 500 m isobath as it defines the typical offshore boundary of the CP jet. During summer months a distinct offshore transport is typical in the vicinity of the CP jet, but peaking just to the north of it at about 33.8°S . The peak offshore flux in this region shifts southward to about 34.25°S during

winter months, reducing toward the north and shifting onshore sooner than during summer months at about 33.75°S . The seasonally differing alongshore pattern of cross-shelf fluxes in the vicinity of the CP jet, suggest differences in jet bifurcation patterns during summer and winter. A similar pattern of significant onshore transport exists during both summer and winter months at between $33.5^{\circ} - 33^{\circ}\text{S}$ and is related to the narrowing of the shelf.

The summer and winter bifurcation of the CP jet is seen in the locations of drifters (Fig. 11) three days after their release from the jet off CP, taken to be a 20 km radius between the 200 and 500 m isobaths off CP in the upper 20 m. 10 000 particles are released every 2 days per month for model years 6, 7 and 8. Every 100th of these particles for all summer (in the case of Fig. 11a) and winter (in the case of Fig. 11b) release experiments are shown as grey dots, the spread of which gives an indication of the intraseasonal variability, while the median positions are shown as black dots. The median location of drifters three days after release during summer months shows two distinct branches of the jet: one that stays on the shelf, centered on the 500 m isobath and the other veers offshore at about 33.8°S , which is consistent with a peak in the offshore transport shown in Fig. 10. During winter (Fig. 11b) two branches of the CP jet are also evident: the more inshore branch is well within the 200-500 m shelf region, while the offshore branch lies somewhat parallel to it, beyond the 500 m isobath, suggesting an earlier divergence of the jet followed by its maintenance in the alongshore direction.

A similar jet separation has been reported off the Oregon coast by Castelao and Barth (2007), who relate it to the intensification of positive wind stress curl equatorward of the cape, which enhances upwelling downstream of the cape, resulting in an intensification of the equatorward velocities. This facilitates the offshore veering of potential vorticity contours and the separation of the jet. During the austral summer upwelling season, the negative wind stress curl intensifies north of Cape Point (enhancing upwelling there) and is accompanied by lines of constant potential vorticity that veer offshore (not shown). This suggests that a similar mechanism is responsible for the offshore veering north of Cape Point

during summer months. However, a more in depth dynamical analysis is required.

Looking at the locations of the drifters ten days after release (Fig. 12), the most noteworthy observation is that more drifters are retained on the shelf in the vicinity of CC and northward, between the 200-500 m isobaths, and more make it into the nearshore domain during winter months. During summer the particles tend to be more dispersed and primarily end up flanking the 500 m isobath in the vicinity of CC and northward revealing that the CP jet primarily feeds the offshore CC jet in summer. On average, 50 % of particles make it to the offshore CC jet (i.e. over the 500 m isobath) per release from the CP jet without being lost off the shelf in summer, while only 15 % make it to the nearshore CC jet region (i.e. over the 200 m isobath). Furthermore, a backtracking drifter experiment (not shown) in which drifters are released from the offshore CC jet in summer months shows that the particles tend to originate from the CP jet region and not the nearshore CC jet. 35 % of particles are dispersed offshore before reaching the CC region during summer as opposed to the 30 % in winter. The difference can be accounted for by strong offshore Ekman transport at the surface during the summer upwelling period and also the greater net offshore transport between the jet and about 33.5° in summer. In winter the particles retained on the shelf feed the whole region between the 200-500 m isobaths off CC and northward.

This lagrangian drifter study has allowed us to visualize the connectivity between the CP jet and the CC jets in a way that is not possible using eulerian methods. It shows that a distinct bifurcation of the CP jet occurs in both winter and summer months. The portion of the jet that remains on the shelf goes on to feed primarily the offshore CC jet during summer and the whole outer-shelf region (between the 200 and 500 m isobaths) during winter.

4. Conclusions

The intense currents over the shelf-edge in the southern Benguela system are known to be crucial in the transport of fish eggs and larvae from their spawning to nursery grounds and have therefore inspired dedicated monitoring effort over the years. While these monitoring programs provide invaluable information on the general characteristics of the jet, it is difficult to re-create a robust climatology of the jet in order to investigate its seasonal signal, nor is it possible to spatially or temporally contextualize the jet in order to better understand its dynamics. We use a climatologically forced model simulation as well as an individual based model in order to resolve the seasonal variability of the jet currents as well as their underlying dynamics.

The results show that although a year-round intensification of surface currents exists off the CP and CC, the intensification is enhanced and extends throughout the shelf-edge region from Cape Agulhas (the southernmost tip of the continent) to CP during the austral spring and summer upwelling season. The bifurcation of the CP jet is clear in the drifter experiments: during both summer and winter months part of the shelf-following CP jet diverges offshore. The double jet feature off CC is clearly resolved in the model, but only during spring and summer months, when the CP jet feeds primarily the offshore branch (over the 500 m isobath) and to a lesser extent the nearshore jet (over the 200 m isobath) that is also amplified by local upwelling off CC. In winter the CP jet stays more confined to the shelf region and goes on to feed the whole shelf region off and northward of CC.

The location (between the 200-500 m isobaths) and intensity ($0.5-0.7 \text{ m}\cdot\text{s}^{-1}$) of the model CP jet is consistent with observed data and, although the model SSTs have a general warm bias throughout the domain, the offshore SST gradients agree well with satellite data. Given that it is the horizontal density gradients, of which SST is a proxy, that drive the alongshore jet currents and given that the upper portion of the jet (0-50 m) correlates very closely to the deep portion (50-500 m) of the jet, we can assume that the surface SST gradient

does indeed provide an excellent proxy for the position and intensity of the jet. Therefore by comparing satellite and model SST gradients we show that while the model reproduces the general timing and intensity of the CP jet quite well, it fails to accurately reproduce the variability of the width and offshore extent of the jet. Satellite data shows that the jet is narrower and closer to the coast than is simulated by the model during the first half of the upwelling season and broader and further offshore during the second half. A heat budget analysis explicitly shows that the intense horizontal temperature gradient is generated by the dichotomy of cooling by mean advection, associated with seasonal upwelling, inshore of about the 350 m isobath and warming by eddy advection, associated with Agulhas influx, offshore of it.

The premise that the jet is geostrophically adjusted is partially confirmed by re-creating the geostrophic velocities using the thermal wind relation and comparing them with model-derived velocities (for both the REF and NOA experiments) that include the influence of non-linearities as well. The geostrophic core of the CP jet is centred over about the 350 m model isobath and is about 40 km wide. Non-linearities associated with Agulhas influx on the offshore side of the jet introduce an additional ageostrophic component and cause it to broaden by about 20 km, at least in its mean manifestation.

The model results have shown us that the geostrophically adjusted system of jet-currents in the southern Benguela associated with upwelling dynamics is modulated both geostrophically and ageostrophically by the influence of the Agulhas as well as by intrinsic variability originating within the upwelling region. Geostrophically, the warm offshore water introduced by the Agulhas enhances the cross-shelf density gradient and thereby enhances the jet and ageostrophically, non-linearities in the form of eddies, rings, filaments and generally enhanced mesoscale variability directly impact the position and intensity of the jet. However, because the model is forced with climatological mean winds and though it can give a sense of intraseasonal intrinsic variability, it cannot provide information on the higher frequency local or remote wind-forced variability. Fig. 13 shows hourly mooring data collected on the SARP line at the location

of the 300 m isobath spanning mid-July 2014 to the beginning of December 2014. It gives a sense of how variable the jet is, persisting for more than a month at times and then complete changes of current direction (from northwest to southeast) occurring within a day. The difficulty with mooring data of course is not knowing whether the jet has shifted slightly to the west or to the east, or if it has actually disappeared. Because of its implication in the success of the southern Benguela fishing industry, there is a particular need for consistent and dedicated monitoring effort, in the form of a more extensive mooring array which captures the cross-shelf structure and variability of the jet. An improved monitoring program together with more realistic model configurations will improve our understanding of the spatial and temporal variability of the shelf-edge jet currents in the southern Benguela.

Acknowledgements

The authors would like to acknowledge the NOAA National Oceanographic Data Centre (NODC) for the production and distribution of the satellite SST products, also thanks to Marcel van den Berg for collection of *in situ* data and assistance with data processing. J.Veitch would like to thank Ross Blamey, Steven Herbette and Julie Deshayes for inspiring discussion and methodological advice. The National Research Foundation (South Africa) is acknowledged for their financial support and the University of Cape Town for their facilities. The authors are grateful to the DEA for the provision of funding and facilities.

References

- Bang, N., Andrews, W., 1974. Direct current measurements of a shelf-edge frontal jet in the southern Benguela system. *Journal of Marine Research* 32, 405–417.
- Boyd, A., Nelson, G., 1998. Variability of the Benguela Current off the Cape Peninsula, South Africa. *South African Journal of Marine Science* 19, 27–39.

- Boyd, A.J.C., Oberholzer, G., 1992. South African Journal of Marine Science: Benguela Trophic Functioning. volume 12. chapter Spatial features of the near-surface and midwater circulation patterns off western and southern South Africa and their role in the life histories of various commercially fished species. pp. 189–206.
- Castelao, R., Barth, J., 2007. The role of wind stress curl in jet separation at a cape. *J. Phys. Oceanogr.* 37, 2652–2671. doi:10.1175/2007JP03679.1.
- Chang, N., 2009. Numerical ocean model study of the Agulhas Bank and the Cool Ridge. Ph.D. thesis. University of Cape Town. South Africa.
- Conkright, M., Locarnini, R., Garcia, H., O'Brien, T., Boyer, T., Stephens, C., Antonov, J., 2002. World Ocean Atlas 2001: objective analyses, data statistics and figures. CR-ROM documentation, Internal Report 17. National Oceanographic Centre. Silver Spring, Md.
- Da Silva, A., Young, C., Levitus, S., 1994. Atlas of surface marine data 1994, vol. 1, Algorithms and procedures, technical report. Technical Report. National Oceanographic and Atmospheric Administration. Silver Spring, Md.
- Debreu, L., Voulard, C., Blayo, E., 2008. AGRIF: Adaptive Grid Refinement in Fortran. *Computational Geosciences* 34.
- Dufois, F., Penven, P., Whittle, C., Veitch, J., 2012. On the warm nearshore bias in Pathfinder monthly SST products over eastern boundary upwelling systems. *Ocean Modelling* .
- Fowler, J., Boyd, A., 1998. Transport of anchovy and sardine eggs and larvae from the western Agulhas Bank to the west coast during the 1993/94 and 1994/95 spawning seasons. *South African Journal of Marine Science* 19, 181–195.
- Haidvogel, D., Beckmann, A., 1999. Numerical Ocean Circulation Modelling. volume 2 of *Environmental Science and Management*. Imperial College Press, London.

- Hoskins, B., 1982. The mathematical theory of frontogenesis. *Annu. Rev. Fluid Mech.* 14.
- Huggett, J., Boyd, A., Hutchings, L., Kemp, A., 1998. Weekly variability of clupeoid eggs and larvae in the Benguela jet current: implications for recruitment. *South African Journal of Marine Science* 19, 197–210.
- J. Butler, 2012. Near-surface hydrography in the region of the Good Hope Jet from 4 years of cruise data.
- Lamont, T., Hutchings, L., van den Berg, M., Goschen, W., Barlow, R., 2015. Hydrographic variability in the St. Helena Bay region of the southern Benguela ecosystem. *Journal of Geophysical Research* 120, 2920–2944.
- Large, W., McWilliams, J., Doney, S., 1994. Oceanic vertical mixing: a review and a model with a nonlocal boundary layer parameterization. *Review of Geophysics* 32, 363–403.
- Lett, C., Verley, P., Mullon, C., Parada, C., Brochier, T., Penven, P., Blanke, B., 2008. A lagrangian tool for modelling ichthyoplankton dynamics. *Environmental Modelling and Software* 23, 1210–1214. doi:10.1016/j.envsoft.2008.02.005.
- van der Lingen, C., Huggett, J., 2003. The role of ichthyoplankton surveys in recruitment research and management of South African anchovy and sardine. , in: Browman, H., Skiftesvik, A. (Eds.), *The Big Fish Bang*. Institute of Marine Research, pp. 303–343.
- Lutjeharms, J., Mathyssen, C., 1995. A recurrent eddy in the upwelling front off Cape Town. *South African Journal of Science* 91, 355–357.
- Lutjeharms, J., Stockton, P., 1987. Kinematics of the upwelling front off Southern Africa., in: Payne, A., Gullard, J., Brink, K. (Eds.), *The Benguela and comparable ecosystems*,. *South African Journal of Marine Science*, pp. 35–49.

- Marchesiello, P., Debreu, L., Couvelard, X., 2008. Spurious diapycnal mixing in terrain-following coordinate models: advection problem and solutions. In preparation: Ocean Modelling .
- Marchesiello, P., McWilliams, J., Scchepetkin, A., 2001. Open boundary conditions for long-term integration of regional oceanic models. Ocean Modelling 3, 1–20.
- Mullon, C., Freon, P., Parada, C., van der Lingen, C., Hugget, J., 2003. From particles to individuals: modelling the early stages of anchovy (*Engraulis capensis/encrasicolus*) in the southern Benguela. Fisheries Oceanography 12, 396–406.
- Nelson, G., 1985. Notes on the physical oceanography of the Cape Peninsula upwelling system. pp. 63–95.
- Nelson, G., Hutchings, L., 1983. The Benguela Upwelling Area. Progress in Oceanography 12.
- Penven, P., Lutjeharms, J., P.Florenchie, 2006. Madagascar: a pacemaker for the Agulhas Current system? Geophysical Research Letters 33.
- Rio, M.H., P.Schaeffer, Lemoine, J.M., F.Hernandez, 2005. Estimation of the Ocean Mean Dynamic Topography through the combination of altimetric data, in-situ measurements and GRACE geoid: from Global to Regional Studies, in: Proceedings of the GOCINA international workshop, Luxembourg.
- Shannon, L., Nelson, G., 1996. The South Atlantic: Present and past circulation. Springer. chapter The Benguela: Large-scale features and processes and system variability. pp. 163–210.
- Shchepetkin, A., McWilliams, J., 1998. Quasi-monotone advection schemes based on explicit locally adaptive dissipation. Monthly Weather Review 126, 1541–1580.

- Shchepetkin, A., McWilliams, J., 2005. The regional oceanic modeling system (ROMS): a split-explicit, free-surface, topography-following-coordinate oceanic model. *Ocean Modelling* 9, 347–404.
- Shchepetkin, A., McWilliams, J., 2008. Handbook of numerical analysis: Computational methods for the ocean and atmosphere.. Elsevier Science. chapter Computational kernel algorithms for fine-scale, multi-process, long-term oceanic simulations. pp. 119–181.
- Shelton, P., Hutchings, L., 1982. Transport of anchovy, *Engraulis capensis* Gilchrist, eggs and early larvae by a frontal jet current. *J.Cons.int.Explor.Mer* 40, 185–198.
- Stenevik, E., Verheye, H., Lipinski, M., Ostrowski, M., Stromme, T., 2008. Drift routes of Cape hake eggs and larvae in the southern Benguela Current system. *Journal of Plankton Research* 30, 1147–1156.
- Strub, P., Shillington, F., James, C., Weeks, S., 1998. Satellite comparison of the seasonal circulation in the Benguela and California Current systems, in: Pillar, S., Moloney, C., Payne, A., Shillington, F. (Eds.), *Benguela Dynamics*. South African Journal of Marine Science. volume 19, pp. 99–112.
- Veitch, J., 2009. Modelling equilibrium dynamics of the Benguela Current system; a numerical modelling approach. . Ph.D. thesis. University of Cape Town.
- Veitch, J., Penven, P., 2017. The role of the agulhas in the benguela current system: A numerical modelling approach. *J. Geophys. Res.* 122. doi:10.1002/2016JC012247.
- Veitch, J., Penven, P., Shillington, F., 2009. The Benguela: a laboratory for comparative studies. *Progress in Oceanography* doi: 10.1016/j.pocean.2009.07.008.

Veitch, J., Penven, P., Shillington, F., 2010. Modeling equilibrium dynamics of the Benguela Current system. *Journal of Physical Oceanography* 40, 1942–1963.

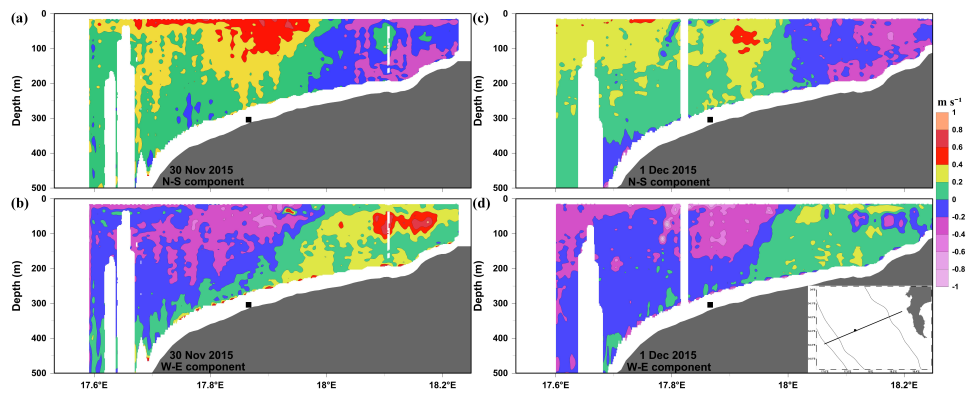


Figure 1: Meridional (top) and zonal (bottom) velocity components of a transect off Cape Point for the 30 November 2015 and 1 December 2015 (left and right respectively). Positive (negative) values are northward and eastward (southward and westward). The black square indicates the position of the ADCP. Units are in m.s^{-1} .

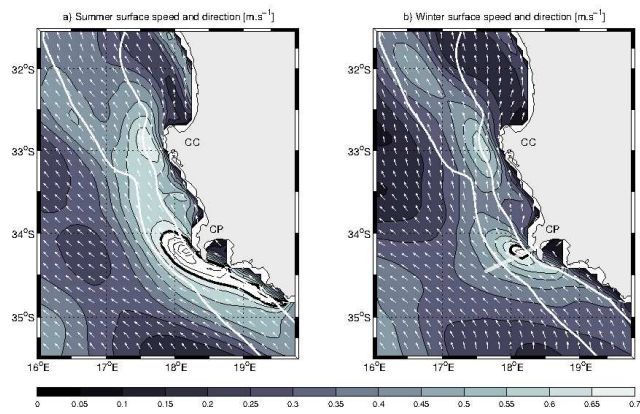


Figure 2: Summer (a) and winter (b) mean model sea surface current speed [$m.s^{-1}$] and direction. The 200 and 500 m isobaths are shown in white and the bold black line is the $0.5m.s^{-1}$ isotach. The contour interval is $0.05m.s^{-1}$. The transparent line in (b) is the location of the SARP line.

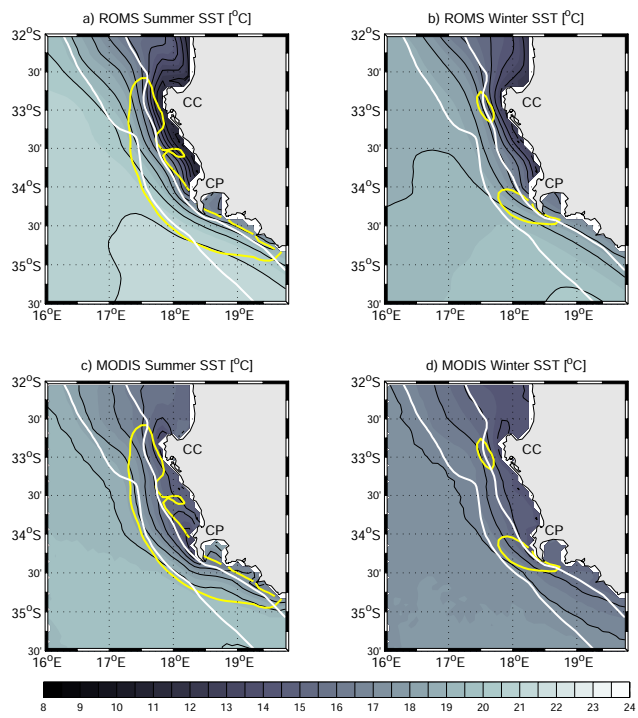


Figure 3: Summer (a,c) and winter (b,d) mean ROMS and satellite SST with the 0.4 m.s^{-1} isotach shown in yellow and the 200 and 500 m isobaths in white.

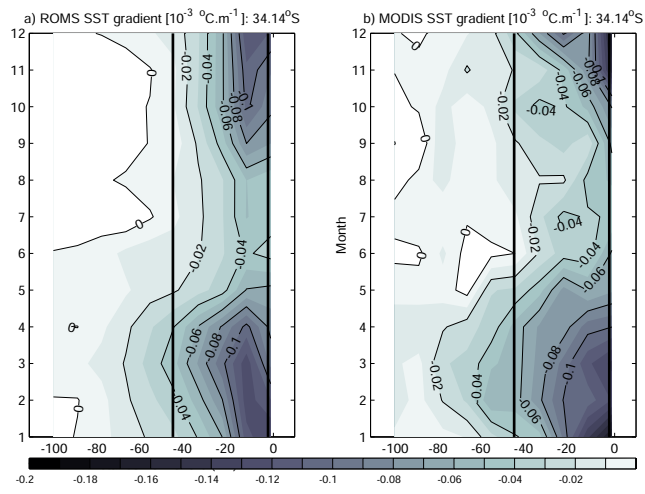


Figure 4: Space-time plot of climatological mean SST gradient across the shelf-edge at 34.14°S for satellite and model data. The 200 and 500 m isobaths are shown as bold lines.

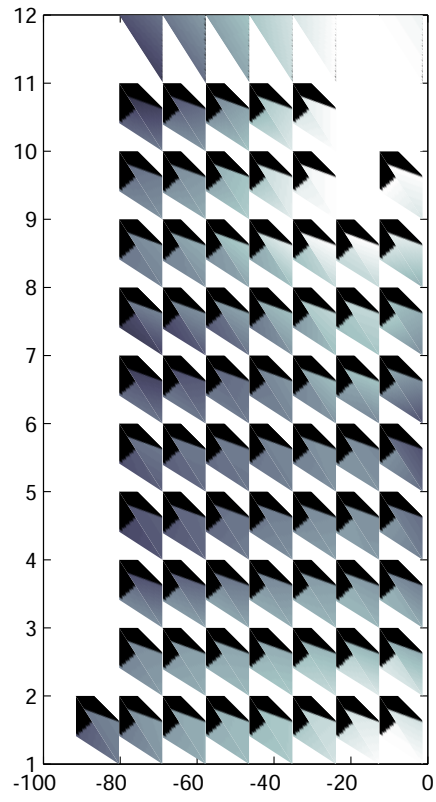


Figure 5: Space-time plot of climatological mean alongshore currents across the shelf-edge at 34.14°S and climatological mean alongshore coastal windstress.

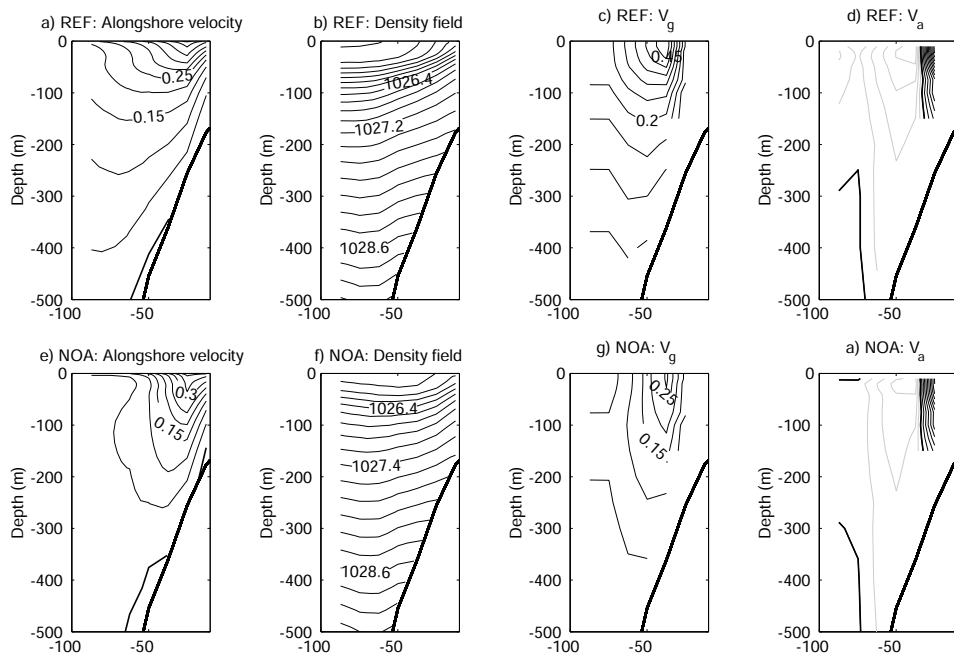


Figure 6: Model-derived alongshore velocity across the shelf-edge at CP, the associated density field, the thermal-wind derived alongshore velocity and the ageostrophic velocity component (the $c.i = 0.5 \text{ m.s}^{-1}$) for the REF and NOA simulations. The grey lines indicating a negative/southward component with a $c.i=0.25 \text{ m.s}^{-1}$ for the ageostrophic component.

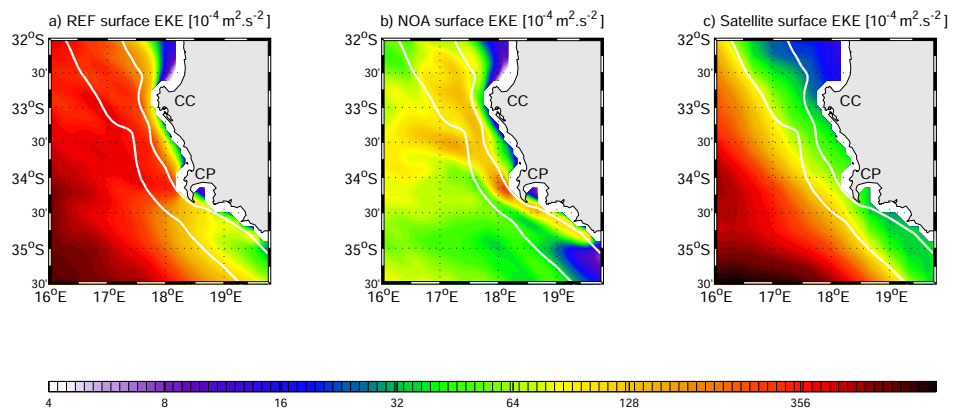


Figure 7: Annual mean surface EKE $[10^{-4} \text{ m}^2 \cdot \text{s}^{-2}]$ for the REF and NOA simulations as well as derived from satellite altimetry.

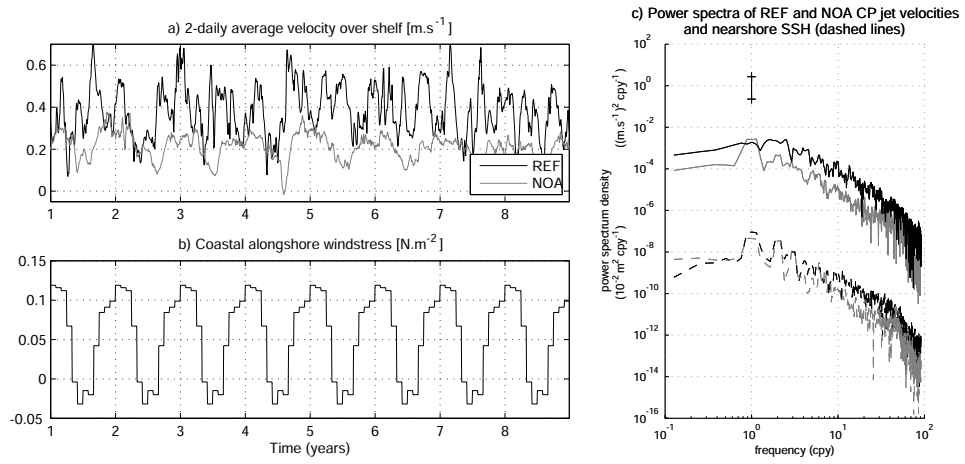


Figure 8: Two-daily across-shelf averaged surface alongshore velocity for the REF and NOA simulations, the corresponding climatological alongshore coastal windstress and the power spectrum density of each of the former as well as the nearshore SSH.

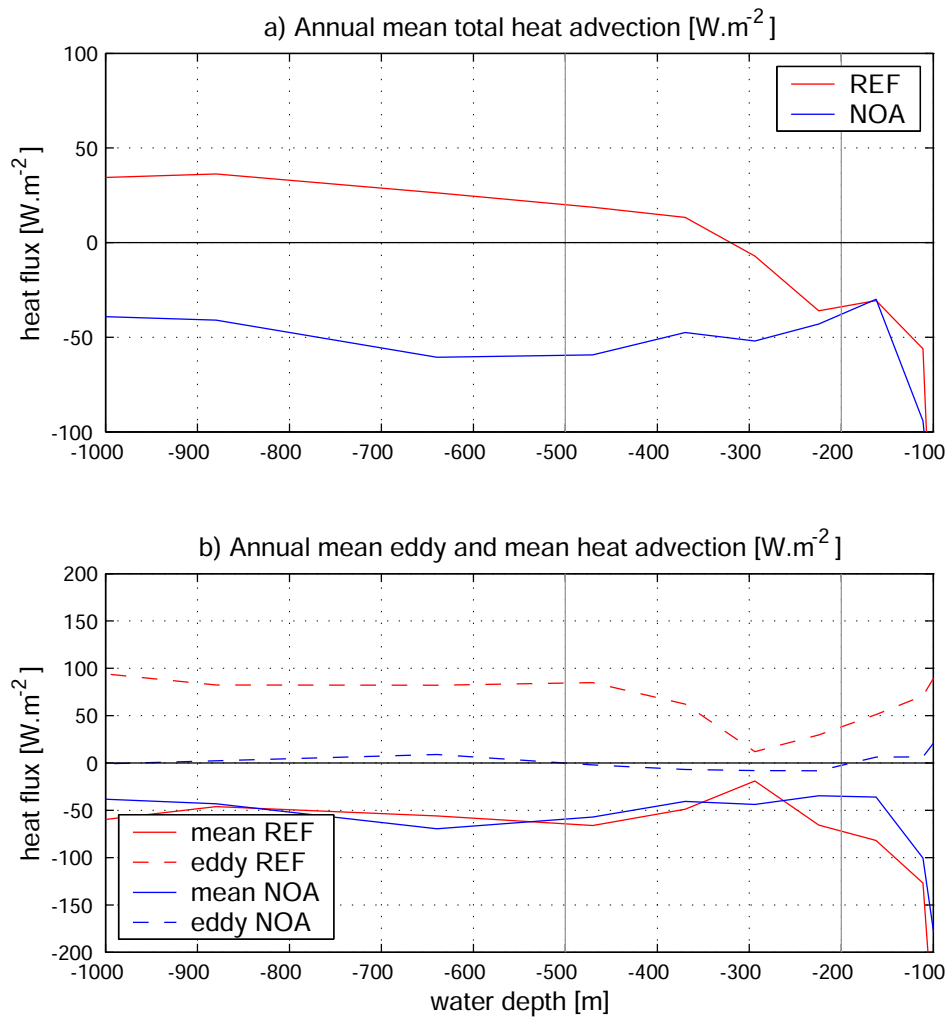


Figure 9: Annual mean depth integrated (0-100 m), alongshore averaged (between 34-33°S) total heat advection and separated into its mean and eddy components for both the REF and NOA simulations across the shelf. The vertical grey lines highlight the 200 and 500 m isobaths.

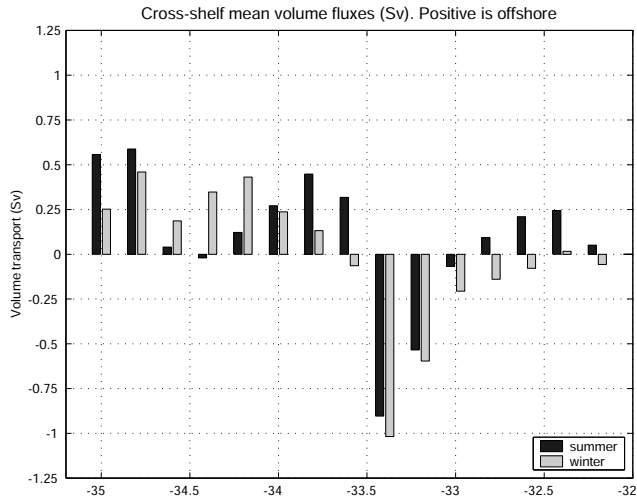


Figure 10: Summer and winter mean cross-shelf (in our context, taken to be the 500 m isobath) volume fluxes, integrated from the surface to 500 m depth and in 0.2° alongshore bins. Positive values indicate an offshore flux.

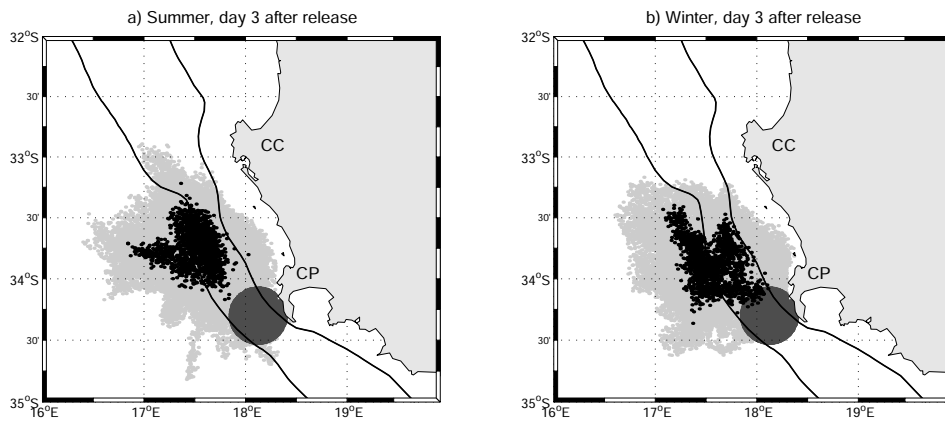


Figure 11: Grey dots indicate locations of every 100th particle three days after release during summer and winter months. The black dots represent the median positions, the dark grey 'halo' is the region of release. The bold black lines represent the 200 and 500 m isobaths.

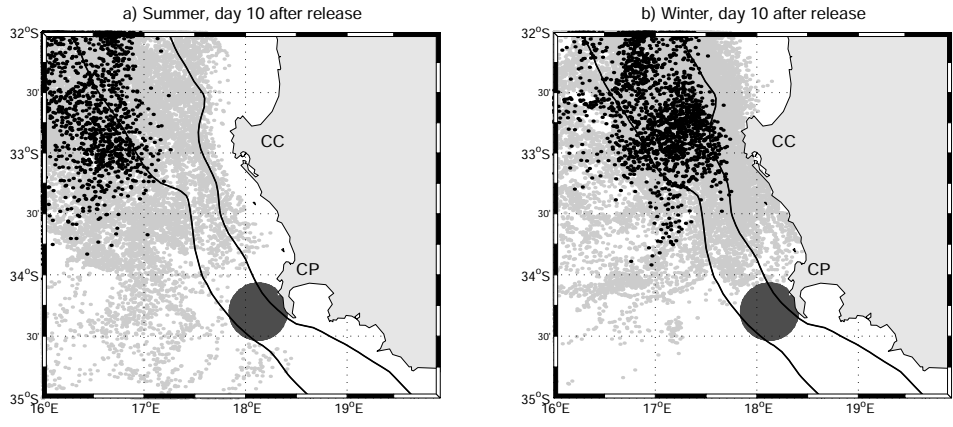


Figure 12: Grey dots indicate locations of every 100th particle ten days after release during summer and winter months. The black dots represent the median positions, the dark grey 'halo' is the region of release. The bold black lines represent the 200 and 500 m isobaths.

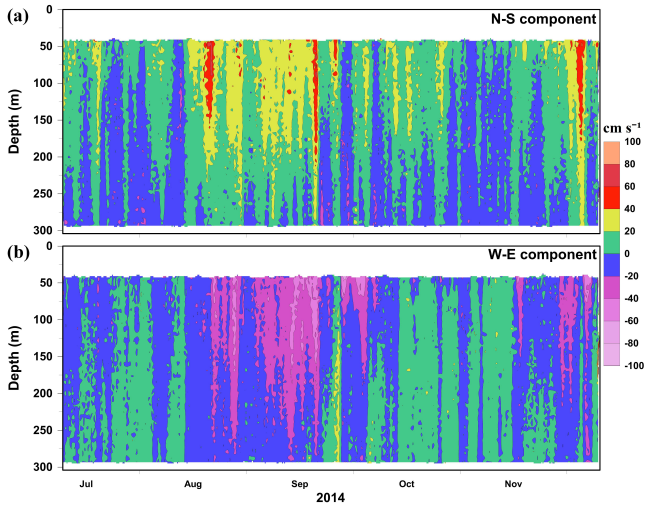


Figure 13: Hourly meridional (top) and zonal (bottom) velocity measurements, spanning July to the beginning of December 2014, from the ADCP (refer to Fig 1) over the shelf-edge. Positive (negative) values are northward and eastward (southward and westward).